Mathematical Model of the Movement of the Human Limbs

Daniel M Dantchev *, Svetoslav Nikolov, Gergana Stefanova Nikolova

Posted Date: 1 October 2025

doi: 10.20944/preprints202510.0029.v1

Keywords: double pendulum; nonlinear dynamics; nonlinear differential equations; biomechanics; chaos; phase diagram; numerical methods; mass-inertial parameters of the human body; mathematical modeling of the human body

 doi:10.20944/preprints202510.0029.v1

Article

Mathematical Model of the Movement of the Human Limbs

Daniel Dantchev [1,2,*], Svetoslav Nikolov [1,3] and Gergana S. Nikolova [1,2]

[1] Institute of Mechanics, Bulgarian Academy of Sciences, Academic Georgy Bonchev St. building 4, 1113 Sofia, Bulgaria
[2] Center of Competence for Mechatronics and Clean Technologies "Mechatronics, Innovation, Robotics, Automation and Clean Technologies" - MIRACle, "Acad. G. Bontchev" Str. 4, 1113 Sofia, Bulgaria
[3] Department of Mechanics, University of Transport, Geo Milev St. 158, 1574 Sofia, Bulgaria
* Correspondence: danieldantchev@gmail.com
† These authors contributed equally to this work.

Abstract

We present a model of the human walking based on the well known model of double pendulum moving in a plane under the influence of g ravity. For constructing the pendulum we use data for the average value of masses of the thigh and shank, as well as for their inertial moments, centers of masses and densities taken from a representative study of the Bulgarian males. We derived the corresponding differential equations governing the model and solved them numerically. We have shown that for moderate initial values of the angles and the angular velocities, describing the system, one has a regular reasonably looking movement of the pendulum resembling that one of the actual walking of humans.

Keywords: double pendulum; nonlinear dynamics; nonlinear differential equations; biomechanics; chaos; phase diagram; numerical methods; mass-inertial parameters of the human body; mathematical modeling of the human body

1. Introduction

The plane double gravitational pendulum serves as a valuable model for understanding the complexities arising from nonlinearity in physical systems. The system's behavior is described by a set of coupled, nonlinear, second-order differential equations that defy analytical solution [1]. Numerical simulation provides a powerful tool for exploring its dynamics, but requires careful attention to numerical errors and energy conservation. The double pendulum's sensitivity to initial conditions and its chaotic nature underscore the limitations of long-term predictability in nonlinear systems. Visualization tools, such as animations and phase space plots, are crucial for analyzing and interpreting the simulation results [2]. In addition to numerically solving the equations we have also used these methods. The numerical exploration of the double pendulum's dynamics reveals its most compelling characteristic: its sensitivity to initial conditions. This sensitivity, a hallmark of chaotic systems, means that infinitesimally small differences in the initial angles or velocities of the pendulums can lead to essentially different trajectories over time [3,4]. The chaotic nature of the double pendulum can be most appealingly visualized through phase space plots. These plots, which map the system's state over time, reveal intricate and often fractal-like structures. Unlike simpler systems with predictable periodic motion that result in closed, repeating loops in phase space, the double pendulum exhibits trajectories that wander seemingly randomly through the phase space, never repeating themselves exactly. This behavior highlights the system's inherent unpredictability and its departure from the predictable dynamics of linear systems.

The current article demonstrates that it can be helpful in matters of biomechanics, which is related to the problems of human walking. We show that within the typical range and parameters

 doi:10.20944/preprints202510.0029.v1

of the human motion the double pendulum behaves relatively regularly and does not have essential chaotic behavior.

The pendulum systems are classical models of nonlinear dynamics [5]. We would like to stress that, generally, the study of the double pendulum is not merely an academic exercise; it holds significance in various scientific and engineering fields [6–13]. Understanding its complexities aids in comprehending the dynamics of multi-body systems, informing the design of robotic arms, satellite stabilization systems, financial modeling, and even contributing to our understanding of planetary motion. Furthermore, it turns helpful for apprehending questions related, as stated, to physics of human motion, and also climate modeling [14,15] (for which Edward Lorenz's coined the famous term "butterfly effect", in article titled "Deterministic Nonperiodic Flow" published in his 1963 paper in the Journal of the Atmospheric Sciences), fundamental physics, and even entertaining sport activities, like golf, namely for modeling the golf swing with double pendulums [16]. The understanding of coupled oscillators is crucial in analyzing the behavior of electrical circuits, mechanical vibrations, and even the rhythmic firing of neurons in the brain.

The planar double gravitational pendulum, a seemingly simple system composed of two pendulums connected in series and swinging under the influence of gravity, belies its deceptive simplicity. It embodies a profound intersection of classical mechanics, nonlinear dynamics, and chaos theory, serving as a potent example of how seemingly deterministic systems can exhibit highly unpredictable behavior. A large number of investigations, both theoretical and experimental, have been dedicated to the problem of determining the chaotic behavior of double pendulum [17–19].

2. The Model

In this section we describe a model of the limbs of the human body. In its simplest version the model represents a type of gravitational pendulum. They can be reduced to plane double or triple gravitational pendulum, i.e., we consider the corresponding limb of the human body to embrace two segments. Any of the branches of the pendulum are supposed to be axis symmetric and characterized by the corresponding densities $\rho_i(s)$, $i = 1, 2$, where s is defined so that it unicly determines the position of the corresponding cross-section of the given branch of the combined.

Of course, we need to determine the Lagrangian of the system. For that we need to clarify what is the kinetic and potential energies of the system in terms of the properly defined variables - see Figure 1. For the total kinetic energy K we obtain consequently

$$K = K_1 + K_2 \tag{1}$$

where K_i, $i = 1, 2$ are the kinetic energies of the segments. Thus, for K_1 one has

$$K_1 = \frac{1}{2}\int_{\{S_1\}} \rho_1(s_1)A(s_1)v_1^2(s_1, t)ds_1, \tag{2}$$

where $\{S_1\}$ is the set of allowed values of $s_1 \in [0, L_1]$ and $A(s_1)$ is the area of the cross-section of segment 1 at position s_1 measured from the beginning of the segment. In what follows we will take the densities of a given segment to be uniform, i.e., $\rho_i(s) = \rho_i$. The last actually reflects the experimental situation - data for the mass densities of a given segment differ from segment to segment, but within the specific segment they are assumed homogeneous. Then, taking into account that

$$v_1^2(s_1, t) = \dot{x}_1^2(s_1, t) + \dot{y}_1^2(s_1, t), \tag{3}$$

and that

$$x_1(s_1, t) = s_1 \sin(\theta_1(t)), \quad \text{and} \quad y_1(s_1, t) = -s_1 \cos(\theta_1(t)), \tag{4}$$

 doi:10.20944/preprints202510.0029.v1

we immediately obtain

$$\dot{x}_1(s_1,t) = s_1\cos[\theta_1(t)]\dot{\theta}_1(t), \quad \text{and} \quad \dot{y}_1(s_1,t) = s_1\sin[\theta_1(t)]\dot{\theta}_1(t), \tag{5}$$

and, therefore

$$v_1^2(s_1,t) = \dot{x}_1^2(s_1,t) + \dot{y}_1^2(s_1,t) = s_1^2\dot{\theta}_1^2(t), \tag{6}$$

which leads to

$$K_1 = \frac{1}{2}\rho_1\int_{\{S_1\}} A(s_1)v_1^2(s_1,t)ds_1 = \frac{1}{2}\rho_1\dot{\theta}_1^2(t)\int_{\{S_1\}} A(s_1)s_1^2 ds_1 = \frac{1}{2}\dot{\theta}_1^2(t)\ I_1. \tag{7}$$

Here

$$I_1 = \rho_1\int_0^{L_1} A(s_1)s_1^2 ds_1 \tag{8}$$

is a moment of inertia of segment "1" about an axes perpendicular to it and centered at its top. We have assumed that the length of the segment is L_1.

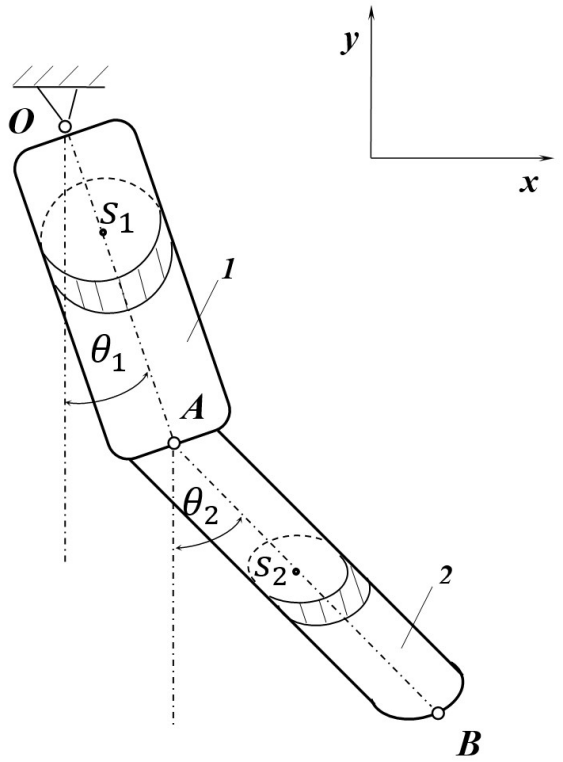

Figure 1. The picture shows a simplified version of the model of either the upper limb, or of the lower limb.

Now we shall deal with the kinetic energy K_2 of the second segment in the limb. Let $s_2 \in [0, L_2]$ is the coordinate along the second segment. Then, looking at the geometry one derives

$$x_2(s_2,t) = L_1\sin\theta_1(t) + s_2\sin\theta_2(t), \tag{9}$$
$$y_2(s_2,t) = -L_1\cos\theta_1(t) - s_2\cos\theta_2(t), \tag{10}$$

which leads to

$$\dot{x}_2(s_2,t) = L_1\cos\theta_1(t)\ \dot{\theta}_1(t) + s_2\cos\theta_2(t)\ \dot{\theta}_2(t), \tag{11}$$
$$\dot{y}_2(s_2,t) = -L_1\sin\theta_1(t)\ \dot{\theta}_1(t) + s_2\sin\theta_2(t)\ \dot{\theta}_2(t), \tag{12}$$

 doi:10.20944/preprints202510.0029.v1

and, therefore, to

$$v_2^2(s_2,t) = L_1^2\dot{\theta}_1^2(t) + s_2^2\dot{\theta}_2^2(t) + 2L_1 s_2 \cos[\theta_1(t)-\theta_2(t)]\ \dot{\theta}_1(t)\dot{\theta}_2(t). \tag{13}$$

Using the above expressions, for the kinetic energy K_2 we derive, consequently:

$$\begin{aligned} K_2 &= \frac{1}{2}\int_{S_2}\rho_2(s_2)A(s_2)v_2^2(s_2,t)ds_2 \\ &= \frac{1}{2}\rho_2\int_{\{S_2\}}[L_1^2\dot{\theta}_1^2(t) + s_2^2\dot{\theta}_2^2(t) + 2L_1 s_2\cos[\theta_1(t)-\theta_2(t)]\ \dot{\theta}_1(t)\dot{\theta}_2(t)] \\ &= \frac{1}{2}L_1^2\dot{\theta}_1^2(t)\left[\int_{\{S_2\}}\rho_2 A(s_2)ds_2\right] + \frac{1}{2}\dot{\theta}_2^2(t)\left[\int_{\{S_2\}}\rho_2 A(s_2)s_2^2 ds_2\right] + L_1\cos[\theta_1(t)-\theta_2(t)]\ \dot{\theta}_1(t)\dot{\theta}_2(t)\left[\int_{\{S_2\}}\rho_2 A(s_2)s_2 ds_2\right] \\ &= \frac{1}{2}m_2L_1^2\dot{\theta}_1^2(t) + \frac{1}{2}I_2\dot{\theta}_2^2(t) + L_1 m_2 C_2\cos[\theta_1(t)-\theta_2(t)]\ \dot{\theta}_1(t)\dot{\theta}_2(t), \end{aligned} \tag{14}$$

where $\{S_2\} \equiv [0, L_2]$,

$$\begin{aligned} m_2 &= \rho_2\int_{\{S_2\}}A(s_2)ds_2, \\ I_2 &= \rho_2\int_{\{S_2\}}s_2^2A(s_2)ds_2, \\ C_2 &= \frac{\int_{\{S_2\}}s_2A(s_2)ds_2}{\int_{\{S_2\}}A(s_2)ds_2}. \end{aligned} \tag{15}$$

Obviously, C_2 is the coordinate of the center of mass of the second segment measured from its beginning.

Summarizing the above, we conclude that, if the limb consists of just two segments, its total kinetic energy $K = K_1 + K_2$ equals to

$$K = \frac{1}{2}\left[I_1 + m_2L_1^2\right]\dot{\theta}_1^2(t) + \frac{1}{2}I_2\dot{\theta}_2^2(t) + L_1m_2C_2\cos[\theta_1(t)-\theta_2(t)]\ \dot{\theta}_1(t)\dot{\theta}_2(t). \tag{16}$$

Now we turn to the potential energy of the system V supposing the bodies to be acted upon by the gravity field of the Earth. Obviously

$$V = V_1 + V_2, \tag{17}$$

where V_1 and V_2 are the potential energies of the segments. From the geometry depicted in Figure 1 one has

$$\begin{aligned} V_1 &= g\int_0^{L_1}\rho_1(s_1)A(s_1)y(s_1)ds_1 \\ &= -g\rho_1\int_0^{L_1}A(s_1)s_1\cos(\theta_1)ds_1 = -g\rho_1\cos(\theta_1)\int_0^{L_1}A(s_1)s_1ds_1 \\ &= -g\cos(\theta_1)m_1C_1, \end{aligned} \tag{18}$$

where

$$C_1 = \frac{\int_0^{L_1}\rho_1 s_1 A(s_1)ds_1}{\int_0^{L_1}\rho_1 A(s_1)ds_1} = \frac{\int_0^{L_1}s_1A(s_1)ds_1}{\int_0^{L_1}A(s_1)ds_1}. \tag{19}$$

In a similar way, for V_2 one derives

$$\begin{aligned} V_2 &= g\int_0^{L_2}\rho_2(s_2)A(s_2)y(s_2)ds_2 \\ &= g\int_0^{L_2}\rho_2(s_2)A(s_2)[-L_1\cos(\theta_1) - s_2\cos(\theta_2)]ds_2 \\ &= -gL_1\cos(\theta_1)\int_0^{L_2}\rho_2(s_2)A(s_2)ds_2 - g\cos(\theta_2)\int_0^{L_2}\rho_2(s_2)s_2A(s_2)ds_2 \\ &= -gm_2[L_1\cos(\theta_1) + \cos(\theta_2)C_2]. \end{aligned} \tag{20}$$

 doi:10.20944/preprints202510.0029.v1

From Equations (18) and (20) we arrive at

$$V = V_1 + V_2 = -g\cos\theta_1(C_1m_1 + L_1m_2) - g\cos\theta_2 C_2 m_2. \tag{21}$$

Once we know the kinetic K and the potential V energies, we derive the Lagrangian $\mathcal{L}$ of the system

$$\begin{aligned}\mathcal{L} = K - V \quad = \quad & \frac{1}{2}\left[I_1 + m_2L_1^2\right]\dot{\theta}_1^2 + \frac{1}{2}I_2\dot{\theta}_2^2 + L_1m_2C_2\cos[\theta_1 - \theta_2]\,\dot{\theta}_1\dot{\theta}_2 \\ & + g(C_1m_1 + L_1m_2)\cos\theta_1 + gC_2m_2\cos\theta_2.\end{aligned} \tag{22}$$

One can also determine the Hamiltonian $\mathcal{H}$ of the system

$$\begin{aligned}\mathcal{H} = K + V \quad = \quad & \frac{1}{2}\left[I_1 + m_2L_1^2\right]\dot{\theta}_1^2 + \frac{1}{2}I_2\dot{\theta}_2^2 + L_1m_2C_2\cos[\theta_1 - \theta_2]\,\dot{\theta}_1\dot{\theta}_2 \\ & - g(C_1m_1 + L_1m_2)\cos\theta_1 - gC_2m_2\cos\theta_2.\end{aligned} \tag{23}$$

Since we did not introduce explicit dependence on the time t, the Hamiltonian of the system is conserved and equal to the stationary energy of the system. According to the standard Hamiltonian formulation, the state of a system is characterized not only by its positions (generalized coordinates) θ_1 and θ_2, but also by its momenta p_1 and p_2. Hence, the Hamiltonian of the system depicted in Figure 1 is:

$$\begin{aligned}H = K + V = \tfrac{I_2}{2\Delta_0}p_1^2 + \tfrac{I_1+m_2L_1^2}{2\Delta_0}p_2^2 - \tfrac{m_2L_1C_2\cos(\theta_1-\theta_2)}{\Delta_0}p_1p_2 \\ -g[(m_1C_1 + m_2L_1)\cos\theta_1 + m_2C_2\cos\theta_2]\,,\end{aligned} \tag{24}$$

where

$$p_1 = \frac{\partial K}{\partial\dot{\theta}_1}\,,\; p_2 = \frac{\partial K}{\partial\dot{\theta}_2}, \text{ and } \Delta_0 = I_1I_2 + m_2I_2L_1^2 - m_2^2L_1^2C_2^2\cos^2(\theta_1 - \theta_2). \tag{25}$$

3. The Equations of Motion

From Equation (22) one obtains the corresponding Euler-Lagrange equations, governing the behavior of the two segments of the considered limb. According to the general theory the equation are to be obtained from

$$\frac{d}{dt}\frac{\partial\mathcal{L}}{\partial\dot{\theta}_i} - \frac{\partial\mathcal{L}}{\partial\theta_i} = 0, \quad i = 1, 2. \tag{26}$$

In this way we obtain a set of two coupled, second-order, nonlinear differential equations:

$$\begin{aligned}& g\sin[\theta_1](C_1m_1 + L_1m_2) + \left(I_1 + L_1^2m_2\right)\ddot{\theta}_1 + C_2L_1m_2\{\dot{\theta}_1\dot{\theta}_2\sin[\theta_1 - \theta_2] \\ & + \ddot{\theta}_2\cos[\theta_1 - \theta_2] - \dot{\theta}_2\left[\dot{\theta}_1 - \dot{\theta}_2\right]\sin[\theta_1 - \theta_2]\} = 0.\end{aligned} \tag{27}$$

and

$$\begin{aligned}& gC_2m_2\sin[\theta_2] + I_2\ddot{\theta}_2 \\ & + C_2L_1m_2\left\{\ddot{\theta}_1\cos[\theta_1 - \theta_2] - \dot{\theta}_1^2\sin[\theta_1 - \theta_2]\right\} = 0.\end{aligned} \tag{28}$$

Equation (27) can be rewritten in the simpler form

$$\begin{aligned}& g\sin[\theta_1](C_1m_1 + L_1m_2) + \left(I_1 + L_1^2m_2\right)\ddot{\theta}_1 \\ & + C_2L_1m_2\left\{\ddot{\theta}_2\cos[\theta_1 - \theta_2] + \dot{\theta}_2^2\sin[\theta_1 - \theta_2]\right\} = 0.\end{aligned} \tag{29}$$

Equations (28) and (29) form the system of two coupled nonlinear differential equations. When modeling the process of walking one shall keep in mind that $\theta_2 \leq \theta_1$, when $\theta_1 > 0$.

 doi:10.20944/preprints202510.0029.v1

In the form of a dynamical model this system is

$$\begin{aligned}\ddot{\theta}_1 &= a_1 - a_2\dot{\theta}_1^2 - a_3\dot{\theta}_2^2,\\ \ddot{\theta}_2 &= -a_4 + a_5\dot{\theta}_1^2 + a_6\dot{\theta}_2^2,\end{aligned} \tag{30}$$

where

$$\begin{aligned}a_1 &= \frac{g}{\Delta_0}\Big[m_2^2C_2^2L_1\cos(\theta_1-\theta_2)\sin\theta_2 - I_2(C_1m_1+L_1m_2)\sin(\theta_1)\Big],\\ a_2 &= \frac{m_2^2C_2^2L_1^2\cos(\theta_1-\theta_2)\sin(\theta_1-\theta_2)}{\Delta_0} = \frac{1}{2}\frac{m_2^2C_2^2L_1^2\sin[2(\theta_1-\theta_2)]}{\Delta_0},\\ a_3 &= \frac{m_2C_2I_2L_1\sin(\theta_1-\theta_2)}{\Delta_0},\\ a_4 &= -\frac{gC_2m_2}{\Delta_0}\{L_1[C_1m_1\sin(\theta_1)\cos(\theta_1-\theta_2)+L_1m_2\cos(\theta_1)\sin(\theta_1-\theta_2)] - I_1\sin(\theta_2)\},\\ a_5 &= \frac{m_2C_2L_1\sin(\theta_1-\theta_2)\big(L_1^2m_2+I_1\big)}{\Delta_0},\\ a_6 &= \frac{1}{2}\frac{m_2^2C_2^2L_1^2\sin[2(\theta_1-\theta_2)]}{\Delta_0},\\ \Delta_0 &= I_1I_2 + m_2L_1^2\Big[I_2 - m_2C_2^2\cos^2(\theta_1-\theta_2)\Big].\end{aligned} \tag{31}$$

The data needed for the evaluation of the above quantities in case of human body are presented in Table 1 on the example of the average Bulgarian males. The data are taken from Ref. [20]. There, actually, the relative location of the center of mass of the body segments are given, but the transformation to physical lengths is trivial. In Ref. [20] one provides data for principal moments of inertia I_{xx}, I_{yy} and I_{zz}, where the coordinate system is centered at the center of mass of the corresponding segment; the z axes is along the segment, while x and y axes for a plane orthogonal to it. Due to the supposed there symmetry, $I_{xx} = I_{yy}$. One way of acting, in order to determine I_1 and I_2 is that they are equal to

$$I_i = (I_{xx} + I_{yy} - I_{zz})/2 + m_ic_1^2, \tag{32}$$

where we are using the Steiner's theorem. Another, direct approach is to recall that the thigh and shank are modeled there as frustum of cones and to derive that for the segment "i" one has

$$I_i = \frac{1}{30}\pi L_i^3\rho_i\Big(R_{i,1}^2 + 3R_{i,1}R_{i,2} + 6R_{i,2}^2\Big), \quad i = 1,2. \tag{33}$$

Let us perform dimensional analysis for the quantities shown in Equation (31). One has that $[\Delta_0] = (kg\times cm^2)^2$. Then $[a_2] = \mathcal{O}(1)$, $[a_3] = \mathcal{O}(1)$, $[a_5] = \mathcal{O}(1)$, and $[a_6] = \mathcal{O}(1)$, i.e., these constants are *dimensionless*. Finally, $[a_1] = s^{-2}$ and $[a_4] = s^{-2}$. We have also to take into account that $g = 9.8\ m/s^2 = 980\ cm/s^2$.

4. Biomechanical Data

In order to apply Equation (33), we have to take into account that, according to Ref. [**?**], for the thigh $R_{1,1} = 9.5\ cm, R_{1,2} = 5.5\ cm, \rho_1 = 1062\ kg/m^3$ while for the shank $R_{2,1} = 5.5\ cm, R_{2,2} = 4.0\ cm$, $\rho_2 = 1088\ kg/m^3$.

 doi:10.20944/preprints202510.0029.v1

Table 1. Geometric and mass-inertial characteristics of the thigh and shank of the average Bulgarian male.

Segment	Length $[cm]$	Mass [kg]	Centre of mass from the proximal end of the segment $[cm]$	Moments of inertia $[kg \times cm^2]$
Thigh	51.0	11.0	21.1	$I_1 = 6321.42$ I_{xx}=1564.0 I_{yy}=1564.0 I_{zz}= 307.7
Shank	37.2	3.3	16.6	$I_2 = 1124.3$ I_{xx}= 231.9 I_{yy}=231.9 I_{zz}= 34.0

Using the values shown in Table 1, one obtains (in standard SI units)

$$\Delta_0 = 0.168 \ - 0.078 \cos^2(\theta_1 - \theta_2). \tag{34}$$

and

$$\begin{aligned}
a_1 &= \frac{56.522 \sin(\theta_1) - 19.216 \cos(\theta_1 - \theta_2) \sin(\theta_2)}{\cos^2(\theta_1 - \theta_2) - 2.147}, \\
a_2 &= -\frac{\sin[2(\theta_1 - \theta_2)]}{2[\cos^2(\theta_1 - \theta_2) - 2.147]}, \\
a_3 &= -\frac{0.402 \sin(\theta_1 - \theta_2)}{\cos^2(\theta_1 - \theta_2) - 2.147}, \\
a_4 &= \frac{81.416 \sin(\theta_1) \cos(\theta_1 - \theta_2) + 59.036 \cos(\theta_1) \sin(\theta_1 - \theta_2) - 43.479 \sin(\theta_2)}{\cos^2(\theta_1 - \theta_2) - 2.1473}, \\
a_5 &= -\frac{5.335 \sin(\theta_1 - \theta_2)}{\cos^2(\theta_1 - \theta_2) - 2.147}, \\
a_6 &= -\frac{\sin[2(\theta_1 - \theta_2)]}{2[\cos^2(\theta_1 - \theta_2) - 2.147]}.
\end{aligned} \tag{35}$$

Note that $a_2 = a_6$ for any θ_1 and θ_2.

The human gait is usually considered as a cycle decomposed into eight phases, see Figure 2. The phases can be categorized in various ways. Here we do that by using the ankles for the hip, knee, and ankle joint, for each of the eight phases of the human gait cycle. The angles are given, i.e. their typical values, in Table 2.

Table 2. The table provides the hip, knee, and ankle joint angles for each of the eight phases of the human gait cycle.

Gait phases of the human gait cycle	Initial contact	Loading response	Mid stance	Terminal stance	Pre Swing	Initial Swing	Mid Swing	Terminal Swing
Hip	20^0	20^0	0^0	-20^0	-10^0	15^0	25^0	20^0
Knee	$0^0 - 5^0$	20^0	$0^0 - 5^0$	$0^0 - 5^0$	40^0	$60^0 - 70^0$	25^0	$0^0 - 5^0$
Ankle joint	0^0	$5^0 - 10^0$	5^0	10^0	15^0	5^0	0^0	0^0

 doi:10.20944/preprints202510.0029.v1

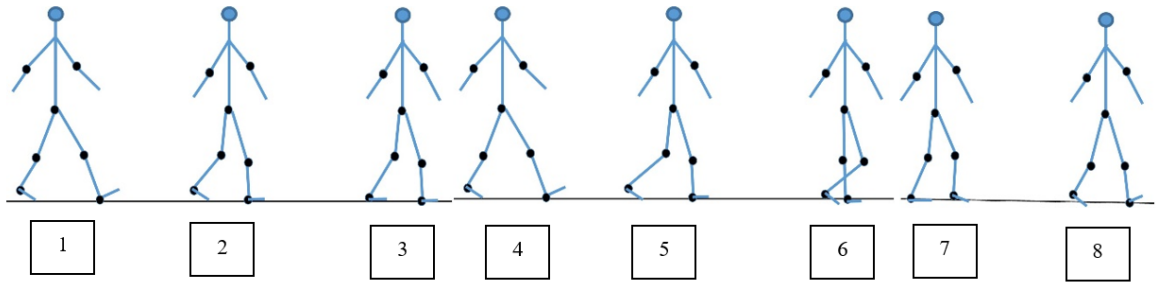

Figure 2. The gait is typically thought of as a continuous series of periodic activities. The full gait cycle is normally defined as the time interval between the first heel strike contact of one foot (for example, the right foot) and the subsequent heel strike contact of the same foot. We use the so-called new gait terms involving the following eight phases, following one of the widely-accepted categorizations reported in the literature: 1) initial contact, 2) loading response, 3) midstance, 4) terminal stance, 5) pre swing, 6) initial swing, 7) mid swing, and 8) late swing, see Refs. [21,22]. All angles are measured with respect to the vertical axis passing trough the middle of the body, see Table 2.

5. Numerical Results

The small free oscillations of a conservative linear system in the phase portrait have the form of closed trajectories in the neighborhood of a stable steady state. It is well-known that amplitudes of oscillations for linear systems (for nonlinear conservative ones also) depend on the initial conditions. On the other hand, its period is permanent and independent of initial conditions and the energy level of the system. The periodic oscillations in conservative systems are always orbitally stable, i.e. for very small perturbations in the initial conditions a periodical motion passes into another one as these two motions are very close.

Solving numerically Equation (30) we obtain:

1) For small initial angles and speeds we obtain the following solutions for θ_1 and θ_2:

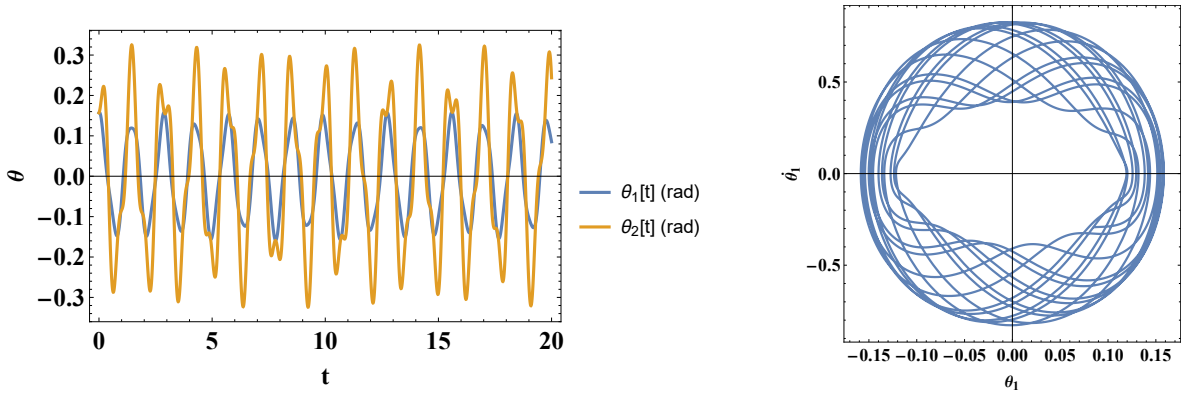

(**a**) (**b**)

Figure 3. (**a**) The figure shows the behavior of θ_1 and θ_2 for $t \in [0, 20]$ and a specific choice of the initial conditions: $\theta_1(0) = 5\pi/100$, $\theta'[0] = 0.1$, $\theta_2[0] = 5\pi/100$, $\theta_2'[0] = 0.1$.(**b**) Phase diagram of the system under the same boundary conditions.

2) For intermediate initial angles and speeds we obtain the following solutions for θ_1 and θ_2:

 doi:10.20944/preprints202510.0029.v1

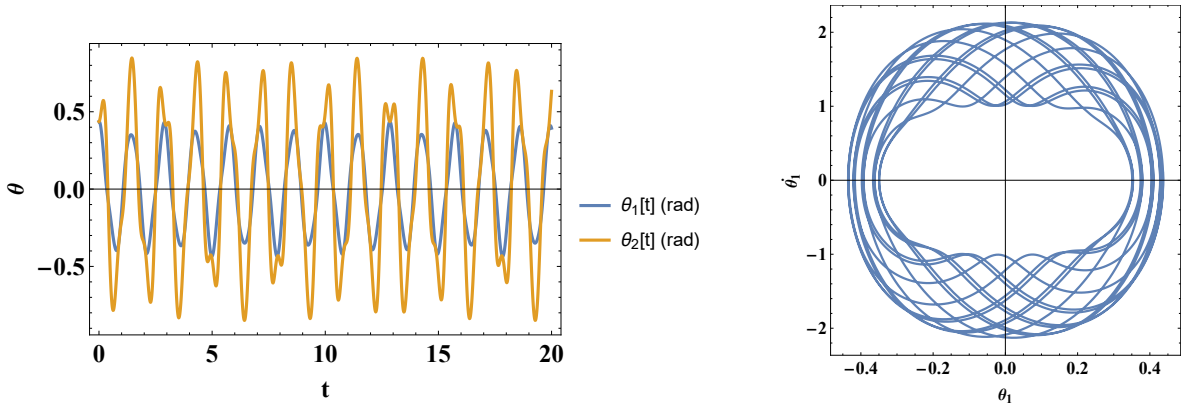

(a) (b)

Figure 4. (**a**) The figure shows the behavior of θ_1 and θ_2 for $t \in [0, 20]$ and a specific choice of the initial conditions: $\theta_1(0) = 5\pi/36$, $\dot{\theta}_1[0] = 0.1$, $\theta_2[0] = 5\pi/36$, $\dot{\theta}_2[0] = 0.1$. (**b**) Phase diagram of the system under the same boundary conditions. It demonstrates that the movement is not purely periodic but there is also an element of chaos in it. We observe that the spread of the phase diagram is about three times larger than for the small angles. i.e., larger the initial angles larger is the spread of the phase diagram.

6. Small Angles Approximation

In the current section we solve both analytically and numerically Equation (28) and Equation (29) form the system of two coupled nonlinear differential equations in the small angles approximation. Performing small angles expansion in these equation and retaining only linear terms, we obtain

$$\ddot{\theta_1}(t) = g\frac{I_2[C_1m_1 + L_1m_2]\,\theta_1(t) - C_2^2L_1m_2\theta_2(t)}{L_1^2m_2\left[C_2^2m_2 - I_2\right] - I_1I_2} \tag{36}$$

and

$$\ddot{\theta_2}(t) = gm_2C_2\frac{\theta_2(t)\left[I_1 + L_1^2m_2\right] - L_1\theta_1(t)[C_1m_1 + L_1m_2]}{L_1^2m_2\left[C_2^2m_2 - I_2\right] - I_1I_2}. \tag{37}$$

Obviously, these two equations describe two linearly coupled oscillators. Looking for a solution in the form

$$\theta_1(t) = A_1\exp[i\omega t], \quad \text{and} \quad \theta_2(t) = A_2\exp[i\omega t] = A_1\,r\,\exp[i\omega t], \quad \text{with} \quad r = A_2/A_1, \tag{38}$$

we obtain

$$\omega = \pm\sqrt{g}\frac{\sqrt{C_1m_1 + L_1m_2}}{\sqrt{L_1m_2(C_2 + L_1) + I_1}}, \tag{39}$$

and

$$r = \frac{(C_1m_1 + L_1m_2)(C_2L_1m_2 + I_2)}{C_2m_2[L_1m_2(C_2 + L_1) + I_1]} = \frac{\omega^2}{g}\frac{C_2L_1m_2 + I_2}{C_2m_2}. \tag{40}$$

Plugging in Equation (39) and Equation (40) the values of all quantities involved, we obtain

$$\omega = \pm 4.709 \quad \text{and} \quad r = 1.618. \tag{41}$$

The behavior of $\theta_1(t)$ and $\theta_2(t)$ is shown in Figure 5. One observes for very small angles periodic behavior. The changes in the behaviors of $\theta_1(t)$ and $\theta_2(t)$ are in phase with each other.

 doi:10.20944/preprints202510.0029.v1

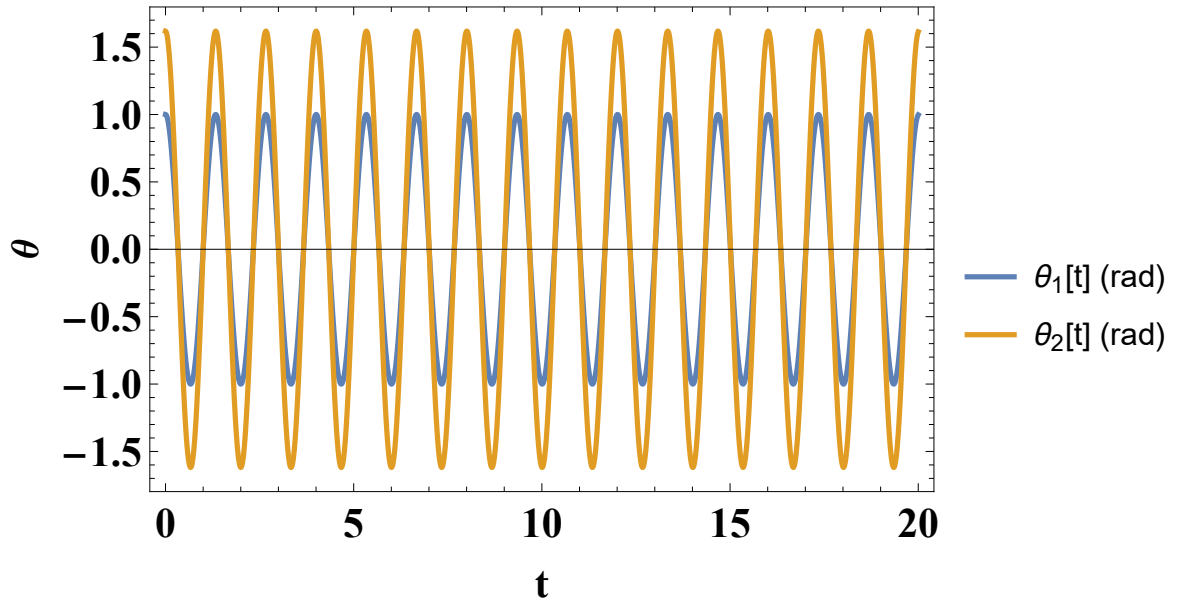

Figure 5. The figure shows the behavior of $\theta_1(t)$ and $\theta_2(t)$ as a function of $t \in [0, 20]$.

7. Comparison of Our Model Results to Real Walking

In this section, we will briefly discuss how our results compare to real walking.

Walking is a fundamental human activity, essential for daily life, work, and social interaction. Its significance extends to well-being, enabling shopping, commuting, and maintaining connections with others. The study of human motion, with a particular focus on gait, has a long history, dating back to ancient times [23]. This research encompasses diverse areas, including neuromuscular disorders, joint replacement, sports injuries, and assistive devices [24,25]. Furthermore, the increasing interest in humanoid and wearable robots [26] underscores the continuing importance of understanding human locomotion.

The results of our model of human walking indicate that for small initial angles (periodic movement), the period $T = 2\pi/\omega \simeq 1.33$ seconds. One forward swing of the leg corresponds to a half cycle, which takes $T_{1/2} = 0.67$ s. This is quite close to the number reported in Ref. [27,28], according to which at slow walk $T_{1/2} \simeq 0.60$ s. $T_{1/2} = 0.67$ s corresponds to about 2400 step/hour. If we assume the average step length to be approximately 0.6 m, we obtain a speed of approximately 1.44 km/h.

For the movements shown in Figure 3, $T_{1/2} = 0.81$ s, while for Figure 4, $T_{1/2} = 0.44$ s. These data correspond to 2.67 km/h and 5.9 km/h, respectively. The corresponding step lengths are, then, $2L\sin(\theta)$. Having that for $T_{1/2} = 0.81$ s one has $\theta = 2 \times 5\pi/100 \simeq 18^\circ$ we obtain for the step length $(L_1 + L_2)\sin(18^\circ) = 0.27$ m and $(L_1 + L_2)\sin(50^\circ) = 0.68$ m for $T_{1/2} = 0.44$ s. According to Ref. [28] [p. 127], see also Refs. [29,30], the speed for a slow walk is about $0.5 m/s = 1.8$ km/h. There one takes a step length of 0.3 m, the time for a step $T_{1/2} \simeq 0.60$ s. For a fast walk, the speed is estimated about $2.0\, m/s = 7.2$ km/h, and the step length of about, 0.7 m, so the step time is about 0.35 s. As we see all these numbers are very close to the numbers we obtained within our model.

8. Conclusions

The mathematical model described in the current article is based on a double pendulum representation of a limb (e.g., thigh + shank) with realistic mass–inertia parameters. The model uses measured anthropometric data (those for average Bulgarian males in the paper). Naturally, it can be tailored to specific populations or individuals, making it a bridge between abstract physics and personalized bio-mechanical solutions. Thus, although it's a theoretical construct, it has clear real-world applications across several domains: *i)* gait analysis and rehabilitation; The model can simulate normal and pathological walking patterns, helping clinicians design targeted physiotherapy or post-surgery recovery plans. *ii)* prosthetics and orthotics design; By adjusting parameters (mass, length, inertia) to match

 doi:10.20944/preprints202510.0029.v1

a patient's anatomy, engineers can optimize artificial limbs for more natural movement. *iii)* injury prevention; Understanding joint loads and motion dynamics can guide ergonomic recommendations for athletes and workers. Many of the biomechanical problems associated with the evolution of total knee and total hip replacements have been evaluated in terms of walking mechanics. Mathematical modeling of human walking is an approach to estimate the human joint kinematics and dynamics during walking. More specifically, mathematical modeling and analysis help us distinguish between healthy patterns and the presence of any pathological alterations.

Summarizing, we conclude that in the current paper, a realistic mathematical model of human limb movement is proposed using a double pendulum that moves in a plane under the influence of gravity. The model simulates the complete limbs of the human body and can easily be scaled to study different groups (children, women and et al.) of human populations. The model is dynamic, and it has a realistic representation, such as a slow/fast healthy walk.

The model can be, obviously, improved by introducing torques acting on the segments of the pendulum. This will lead to source terms on the right-hand side of Equation (28) and Equation (29). The problem will become even more interesting and complicated if these torques depend on the time [31]. Understanding torques enables inferences about the muscles that most likely contract at certain moments to cause the leg to swing in tandem with gravity [24]. In addition, one can also consider a double inverted pendulum [32–35].

As already stated above, the key characteristic of the model is its non-linearity and chaos. Small changes in initial conditions can lead to different outcomes. This makes it a powerful model for studying the complex control required for human movement [9,31,36].

The double pendulum is a cornerstone model for understanding how the human body moves, as it perfectly illustrates the mechanics of multi-segment chains. Much of our gait (walking/running) can be explained by passive pendulum-like motion, which is incredibly energy-efficient. The model helps us understand this: indeed, during the swing phase of walking or running, the leg behaves remarkably like a double pendulum.

Author Contributions: Conceptualization, D.D., S.N. and G.N.; methodology, D.D., S.N. and G.N.; software, D.D.; validation, D.D., S.N. and G.N.; formal analysis, D.D. and S.N.; investigation, D.D., S.N. and G.N.; resources, D.D., S.N. and G.N.; data curation, G.N; writing—original draft preparation, D.D. and G.N.; writing—review and editing, D.D., S.N. and G.N.; visualization, D.D.; All authors have read and agreed to the published version of the manuscript.

Funding: This work is supported by Grant KP-06-H72/5, competition for financial support for basic research projects—2023, Bulgarian National Science Fund.

Data Availability Statement: No new data were created in the current article.

Acknowledgments: This work was accomplished by the Center of Competence for Mechatronics and Clean Technologies "Mechatronics, Innovation, Robotics, Automation and Clean Technologies" – MIRACle, with the financial support of contract No. BG16RFPR002-1.014-0019-C01, funded by the European Regional Development Fund (ERDF) through the Programme "Research, Innovation and Digitalisation for Smart Transformation" (PRIDST) 2021–2027.

Conflicts of Interest: The authors declare no conflicts of interest.

References

1. Ott, E. *Chaos in dynamical systems*; Cambridge university press, 2002.
2. Rose, J.; Gamble, J.G. Human walking. *Philadelphia* **2006**.
3. Kim, S.Y.; Hu, B. Bifurcations and transitions to chaos in an inverted pendulum. *Phys. Rev. E* **1998**, *58*, 3028.
4. DeSerio, R. Chaotic pendulum: The complete attractor. *Am. J. of Phys.* **2003**, *71*, 250–257.
5. Nayfeh, A.H.; Mook, D.T. *Nonlinear oscillations*; John Wiley & Sons, 2024.
6. Strogatz, S.H. *Nonlinear Dynamics and Chaos: With Applications to Physics, Biology, Chemistry, and Engineering*; Chapman and Hall/CRC, 2024. https://doi.org/10.1201/9780429398490.

 doi:10.20944/preprints202510.0029.v1

7. Ardema, M.D. *Analytical dynamics: theory and applications*; Springer Science & Business Media, 2005.
8. Guckenheimer, J.; Holmes, P. *Nonlinear oscillations, dynamical systems, and bifurcations of vector fields*; Vol. 42, Springer Science & Business Media, 2013.
9. Baker, G.L.; Blackburn, J.A. *The pendulum: a case study in physics*; OUP Oxford, 2008.
10. Dutra, M.S.; de Pina Filho, A.C.; Romano, V.F. Modeling of a bipedal locomotor using coupled nonlinear oscillators of Van der Pol. *Biological Cybernetics* **2003**, *88*, 286–292.
11. Nikolov, S.G.; Vassilev, V.M.; Zaharieva, D.T. Analysis of swing oscillatory motion. In Proceedings of the Annual Meeting of the Bulgarian Section of SIAM. Springer, 2018, pp. 313–323.
12. Nikolov, S.; Zaharieva, D. Dynamical behaviour of a compound elastic pendulum. In Proceedings of the MATEC Web of Conferences. EDP Sciences, 2018, Vol. 145, p. 01003.
13. Arnold, V.I. *Geometrical methods in the theory of ordinary differential equations*; Vol. 250, Springer Science & Business Media, 2012.
14. Baines, P.G. Lorenz, EN 1963: Deterministic nonperiodic flow. Journal of the Atmospheric Sciences 20, 130–41.1. *Progress in Physical Geography* **2008**, *32*, 475–480.
15. Lorenz, E.N. Deterministic nonperiodic flow 1. In *Universality in Chaos, 2nd edition*; Routledge, 2017; pp. 367–378.
16. Penner, A.R. The physics of golf. *Reports on progress in physics* **2002**, *66*, 131.
17. Shinbrot, T.; Grebogi, C.; Wisdom, J.; Yorke, J.A. Chaos in a double pendulum. *American Journal of Physics* **1992**, *60*, 491–499.
18. Levien, R.; Tan, S. Double pendulum: An experiment in chaos. *American Journal of Physics* **1993**, *61*, 1038–1038.
19. Komuro, M. Double pendulum and chaos. *Journal of the Robotics Society of Japan* **1997**, *15*, 1104–1109.
20. Nikolova, G.S.; Toshev, Y.E. Estimation of male and female body segment parameters of the Bulgarian population using a 16-segmental mathematical model. *Journal of biomechanics* **2007**, *40*, 3700–3707.
21. Nikolova, G.; Kotev, V.; Dantchev, D.; Tsveov, M. Study of mass-inertial characteristics of female human body by walking. In Proceedings of the AIP Conference Proceedings. AIP Publishing LLC, 2020, Vol. 2239, p. 020032.
22. Nikolova, G.; Dantchev, D.; Tsveov, M. Age changes of mass-inertial parameters of the female body by walking. *Vibroengineering Procedia* **2023**, *50*, 125–130.
23. Harris, G.F.; Smith, P.A.; et al. Human motion analysis: current applications and future directions. *(No Title)* **1996**.
24. Braune, W.; Fischer, O. *The human gait*; Springer Science & Business Media, 2012.
25. Winter, D.A. *Biomechanics and motor control of human movement*; John wiley & sons, 2009.
26. Asbeck, A.T.; De Rossi, S.M.; Galiana, I.; Ding, Y.; Walsh, C.J. Stronger, smarter, softer: next-generation wearable robots. *IEEE Robotics & Automation Magazine* **2014**, *21*, 22–33.
27. Herman, I.P. *Physics of the human body*; Springer, 2007.
28. Herman, I.P. *Physics of the human body*; Springer, 2007. https://doi.org/10.1007/978-3-319-23932-3.
29. Majed, L.; Ibrahim, R.; Lock, M.J.; Jabbour, G. Walking around the preferred speed: examination of metabolic, perceptual, spatiotemporal and stability parameters. *Frontiers in physiology* **2024**, *15*, 1357172.
30. Saibene, F.; Minetti, A.E. Biomechanical and physiological aspects of legged locomotion in humans. *European journal of applied physiology* **2003**, *88*, 297–316.
31. Chen, J. Chaos from simplicity: an introduction to the double pendulum **2008**.
32. Buczek, F.L.; Cooney, K.M.; Walker, M.R.; Rainbow, M.J.; Concha, M.C.; Sanders, J.O. Performance of an inverted pendulum model directly applied to normal human gait. *Clinical Biomechanics* **2006**, *21*, 288–296.
33. Colobert, B.; Crétual, A.; Allard, P.; Delamarche, P. Force-plate based computation of ankle and hip strategies from double-inverted pendulum model. *Clinical biomechanics* **2006**, *21*, 427–434.
34. Carroll, S.; Owen, J.S.; Hussein, M.F. Experimental identification of the lateral human–structure interaction mechanism and assessment of the inverted-pendulum biomechanical model. *Journal of Sound and Vibration* **2014**, *333*, 5865–5884.
35. Kuo, A.D. The six determinants of gait and the inverted pendulum analogy: A dynamic walking perspective. *Human movement science* **2007**, *26*, 617–656.
36. Morin, D. *Introduction to classical mechanics: with problems and solutions*; Cambridge University Press, 2008.